

Andreev-reflection spectroscopy in neutron-irradiated Mg^{11}B_2

D. Daghero,¹ A. Calzolari,¹ G.A. Ummarino,¹ M. Tortello,¹ R.S. Gonnelli,¹
V.A. Stepanov,² C. Tarantini,³ P. Manfrinetti,⁴ and E. Lehmann⁵

¹*Dipartimento di Fisica and CNISM, Politecnico di Torino, 10129 Torino, Italy*

²*P.N. Lebedev Physical Institute, Russian Academy of Sciences, 119991 Moscow, Russia*

³*CNR-INFM-LAMIA and Dipartimento di Fisica, Università di Genova, 16146 Genova, Italy*

⁴*CNR-INFM-LAMIA and Dipartimento di Chimica e Chimica Industriale, Università di Genova, 16146 Genova, Italy*

⁵*Paul Scherrer Institut, Dept. Spallation Neutron Source SINQ, CH-5232 Villigen, Switzerland*

We report on recent results of point-contact spectroscopy measurements in Mg^{11}B_2 polycrystals irradiated at different neutron fluences up to $\Phi = 1.4 \cdot 10^{20} \text{ cm}^{-2}$. The point contacts were made by putting a small drop of Ag paint – acting as the counterelectrode – on the cleaved surface of the samples. The gap amplitudes were extracted from the experimental conductance curves through a two-band Blonder-Tinkham-Klapwijk fit and reported as a function of the critical temperature of the junctions, T_c^A . The resulting $\Delta_\sigma(T_c^A)$ and $\Delta_\pi(T_c^A)$ curves show a clear merging of the gaps when $T_c^A \simeq 9 \text{ K}$ that perfectly confirms the findings of specific-heat measurements in the same samples. Anomalous contacts with $T_c^A > T_c$ (being T_c the bulk critical temperature) were often obtained, particularly in samples irradiated at very high fluences. Their fit gave a different dependence of Δ_π on T_c^A . The possible reasons of this unusual behavior are discussed in terms of short-range inhomogeneities and/or local current-induced annealing.

PACS numbers: 74.45.+c, 74.70.Ad, 74.62.Dh

I. INTRODUCTION

Most of the present fundamental research on the two-band superconductor MgB_2 is devoted to studying the effects of substitutions and disorder on its properties. This interest in exploring the “neighborhood” of the pure compound is justified in part by the quest of a recipe for improving some of its properties – especially in view of power or electronic applications – and in part by the need of understanding at the best this unique example of two-band phonon-mediated superconductor with a relatively high T_c . As a matter of fact, the presence of two systems of bands crossing the Fermi surface, each developing an energy gap below T_c , has a number of intriguing consequences that make the physics of MgB_2 unexpectedly rich and complex. One of these aspects is the role of scattering by impurities. Due to the different parity of the σ and π bands, scattering of quasiparticles *between* them is highly improbable in the pure compound, while almost independent scattering rates exist *within* the bands. Intraband scattering has no effect on the gaps or on T_c , but affects various properties of the material, e.g. the critical field¹ and the magnetic-field dependence of the gaps². On this basis, the ratio of the diffusivities in the two bands has been experimentally evaluated in pure MgB_2 ^{3,4,5}.

According to an early prediction of the two-band model⁶, the increase of interband scattering in a system like MgB_2 should make the two gaps approach each other and finally merge into a single BCS gap. However, observing this effect in a real material has turned out to be more difficult than expected. The few chemical substitutions that actually take place (e.g. C substitution for B, Al or Mn substitution for Mg) give rise to lattice or electronic effects that can mask the increase in disorder. For example, C and Al substitutions also cause remarkable

changes in the DOS at the Fermi level, in the phonon frequencies, in the cell volume and so on, with an obvious complication in the interpretation of the data. In C-substituted single crystals the merging of the gaps has been recently observed⁷ as arising from the interplay of the band filling due to electron doping and an increasing amount of interband scattering, probably due to extrinsic reasons^{8,9}.

The controlled damaging of the compound by means of irradiation allows partly overcoming these difficulties, even though the irradiated material is far from being an “ideal” disordered version of MgB_2 . In particular, side effects of irradiation are the creation of Li atoms and He nuclei in the lattice (due to the thermal neutron capture by ^{10}B nuclei), the reduction in the partial DOS of the $2p_{x,y}$ states¹⁰, the anisotropic expansion of the crystal lattice¹¹. The effect of neutron irradiation (up to very high fluences) on the energy gaps of MgB_2 has been recently studied by means of specific-heat measurements¹², showing the achievement of single-gap superconductivity in samples with T_c as low as 11 K.

In this paper, we present and discuss the results of point-contact spectroscopy measurements in the same neutron-irradiated Mg^{11}B_2 samples studied in Ref. 12. We will show that the gap amplitudes measured by PCS agree very well with those given by specific-heat measurements and we will discuss the experimental trend of the gaps within the two-band Eliashberg theory.

Moreover, we will report on the anomalous features of a large number of contacts whose Andreev critical temperature T_c^A is greater than the bulk T_c . These contacts feature very good Andreev-reflection conductance curves that were very well fitted by the two-band Blonder-Tinkham-Klapwijk (BTK) model to extract the gap amplitudes Δ_σ and Δ_π . Once reported as a function

of T_c^A , Δ_π has a completely different trend with respect to that reported in Ref. 12 and observed by PCS in “standard” contacts. We will discuss this odd result in terms of local nanoscale inhomogeneities of the material and/or local annealing due to the technique we used to tune the properties of our “soft” point-contact junctions.

II. EXPERIMENTAL DETAILS

The procedure for sample fabrication and irradiation is reported in detail elsewhere^{11,12}. The samples were prepared by direct synthesis from pure elements, using in particular isotopically-enriched ^{11}B (99.95% purity) with a residual ^{10}B concentration lower than 0.5% so as to make the penetration depth of thermal neutrons greater than the sample thickness¹². The samples we measured had been irradiated at the Paul Scherrer Institute (PSI) in Villigen, Switzerland. For simplicity and ease of comparison, let us label them as in Ref.12, i.e. P0 (pristine Mg^{11}B_2), P3 (fluence $\Phi = 7.6 \cdot 10^{17}\text{cm}^{-2}$), P3.7 ($\Phi = 5.5 \cdot 10^{18}\text{cm}^{-2}$), P4 ($\Phi = 1.0 \cdot 10^{19}\text{cm}^{-2}$) and P6 ($\Phi = 1.4 \cdot 10^{20}\text{cm}^{-2}$). Many of their structural and transport properties are reported in Refs. 11 and 12. The bulk critical temperatures, defined as $T_c \equiv T_{90\%}$ of the superconducting transition measured by susceptibility, are: 38.8 K for P0, 35.6 K for P3, 25.8 K for P3.7, 20.7 K for P4, 8.7 K for P6. The width of the superconducting transition, defined as $\Delta T_c(10\% - 90\%)$, varies from 0.3 K (in P0 and P3) up to a maximum of 0.9 K (in sample P4)¹². The transition remains rather sharp also in the most irradiated sample, which indicates a highly homogeneous defect distribution even at the highest fluence. This homogeneity is also confirmed by the sharp X-ray diffraction peaks for the (002) and (110) reflections reported in Ref. 13, which also indicate an anisotropic expansion of the cell parameters, more pronounced along the c axis (up to 1%). The residual resistivity increases by two orders of magnitude (from 1.6 $\mu\Omega\cdot\text{cm}$ for P0 to 130 $\mu\Omega\cdot\text{cm}$ for P6) with a corresponding reduction in the residual resistivity ratio (RRR).

The point contacts were made by placing a small drop of silver paint on the freshly cleaved surface of the samples¹⁴. The conductance curves, dI/dV vs. V , were obtained by numerical differentiation of the measured $I - V$ curve. In all cases, we studied the temperature dependence of the curves, which show clear Andreev-reflection features, so as to determine the critical temperature of the junction (in the following referred to as the “Andreev critical temperature”, T_c^A). Strictly speaking, in fact, T_c^A rather than the bulk T_c is the critical temperature to be related to the local gap amplitudes measured in a given contact. In point-contact spectroscopy, T_c^A can correspond to any temperature between the onset and the completion of the superconducting magnetic transition. Therefore, one usually has $T_c^A = T_c$ within the experimental broadening of the superconducting transition, i.e. $T_{0\%} \leq T_c^A \leq T_{100\%}$ (let us recall that here we

defined $T_c \equiv T_{90\%}$). In irradiated samples, this actually occurs in a subset of contacts we will call “standard” contacts. The conductance curves were divided by the normal-state conductance and then fitted with a two-band BTK model in which the conductance through the junction is expressed by $G = (1 - \omega_\pi)G_\sigma + \omega_\pi G_\pi$, G_σ and G_π being the partial σ - and π -band conductances, and ω_π the weight of the π -band contribution^{14,15}. The model contains as adjustable parameters the gap amplitudes Δ_σ and Δ_π , the barrier parameters Z_σ and Z_π , the phenomenological broadening parameters Γ_σ and Γ_π , plus the weight w_π . The broadening parameters enter in the definition of the density of states in the usual way, i.e.

$$N(E) = \Re \left(\frac{E - i\Gamma}{\sqrt{(E - i\Gamma)^2 - \Delta^2}} \right).$$

In this context, they account for both intrinsic (i.e. finite lifetime of quasiparticles) and extrinsic (related to the technique and the nature of the contacts) phenomena that smear out the conductance curves. $Z_{\sigma,\pi}$ are related to the potential barrier height at the interface and to the mismatch in the Fermi velocity v_F between the two sides of the contact. Owing to the different values of v_F in the σ and π bands, we allow $Z_\sigma \neq Z_\pi$. Finally, w_π is predicted to range from 0.66 to 0.99 for perfectly directional tunneling in pure MgB_2 ¹⁶, depending on the angle of current injection with respect to the ab planes. In the absence of specific predictions in samples with reduced anisotropy, we kept w_π in the same range as in Refs. 3,14.

We generally selected contacts with rather high resistance and, especially, with no dips¹⁷ in the conductance curves, so as to ensure the fulfillment of the conditions for ballistic conduction¹⁸. When the contact resistance was too small, or its conductance did not show clear Andreev-reflection features, we were able to change the contact characteristics (in a surprisingly repeatable way) by applying short voltage or current pulses to the junction itself. In some cases, we also used the magnetic field to clarify whether one or two gaps were present, as explained in detail elsewhere¹⁴ and in the following.

III. RESULTS IN STANDARD CONTACTS

Fig. 1 reports an example of the raw conductance curves measured as a function of the temperature in three point contacts made on samples P3, P4 and P6. The low-temperature curves clearly show the typical Andreev-reflection features – in particular, the two symmetric maxima at $\pm V_{\text{peak}}$ approximately corresponding to the edges of the small gap. The large gap-features are usually less clear even in pure MgB_2 ¹⁴ and in disordered samples they are difficult to see. The thick curve in each panel indicates the normal-state conductance and the relevant temperature is thus chosen as the T_c^A of the contacts.

Note that, in all cases, T_c^A lies between the begin and the end of the magnetic superconducting transition.

In Fig. 1(a) and (b) the shape of the normal-state conductance curves and the absence of dips¹⁷ in the superconducting state indicate that no heating occurs in the junctions, which are thus in the ballistic regime – i.e., the contact size a is smaller than the mean free path ℓ – and energy-resolved spectroscopy is possible. In Fig. 1(c) small dips at $|V| > |V_{\text{peak}}|$ suggest that the contact might actually be in the diffusive regime (i.e. $\ell_e < a < \Lambda$, being ℓ_e the elastic mean free path and Λ the diffusion length¹⁸) in which energy-resolved spectroscopy is still possible. In this regime, the resistance of a point contact between two normal metals – in the hypothesis that the Fermi velocity of the metals are almost equal and the resistivity of one metal (here Ag) is much smaller than the resistivity of the other (here sample P6) – can be expressed by¹⁹

$$R_N = \frac{4\rho\ell}{3\pi a^2} + \Gamma(k) \frac{\rho}{4a} \quad (1)$$

where the first term is the Sharvin resistance for ballistic conduction and the second one is the Maxwell resistance for the thermal regime multiplied by a function of the Knudsen ratio $k = \ell/a$. This function, Γ , is always of the order of unity. ρ is the normal-state resistivity of the irradiated sample (that we will identify with the residual resistivity) and ℓ is the mean free path (evaluated in Ref.13). In the second term, the contribution of the first half of the contact (the Ag counterelectrode) has been neglected^{20,21} due to the much smaller resistivity of Ag with respect to that of sample P6. At $T < T_c$ the irradiated MgB₂ is superconducting and, thus, the contribution of the second term in eq. 1 should disappear. Nevertheless, it is easy to show that even at very low bias voltages – of the order of the energy gap, here about 1 meV as we will discuss later – the current density in the contact is higher than the critical current density and thus tends to drive normal a small volume of the superconductor pushing back the NS boundary a short distance²². If the size of this normal region is smaller than the coherence length the spectroscopy of the gap is still possible²³, but the second term in eq. 1 starts playing a role and a small, voltage-dependent and temperature-dependent heating appears in the contact. The small vertical shift in the conductance curves shown in Fig. 1(c) on increasing temperature confirms this picture indicating that the temperature-dependent resistivity of the material plays a role in the contact resistance. However, heating of the contact region generally gives rise to an apparent decrease of the critical temperature of the contact T_c^A with respect to the bulk T_c . Here the superconducting features disappear at some temperature between 8.0 and 8.5 K, which is only slightly smaller than $T_c = 8.7$ K. Hence, we can conclude that a very moderate heating is likely to occur in the contact shown in Fig. 1(c) and it can be safely neglected as long as the voltage drop across the junction is of the order of V_{peak} . We will show in greater detail in Section V A that the two conditions described

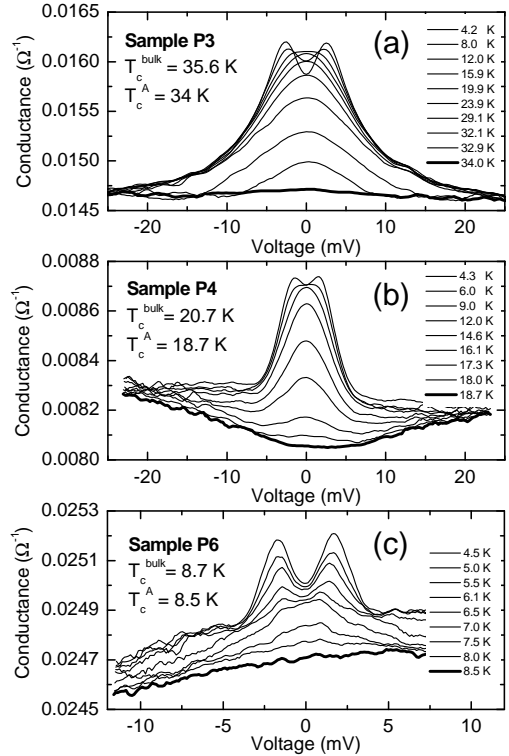


FIG. 1: Temperature dependence of the raw conductance curves measured in three contacts on samples P3, P4 and P6, whose bulk critical temperature is indicated. Thicker lines indicate the normal-state conductance, which, in most of the contacts, is practically temperature-independent and is reached when $T = T_c^A$. The temperature of each curve is also indicated in the legend.

above (normal-region size $< \xi$ and very small heating) are compatible with the curves shown in Fig. 1(c) only if parallel diffusive nanocontacts are supposed to be present in the contact region.

Fig. 2 reports an example of experimental, normalized conductance curve (symbols) for each sample. Notice that the horizontal scale is the same for all the panels, so as to highlight the shrinking of the Andreev-reflection structures on increasing the neutron fluence – which indicates, in turn, a decrease in the amplitude of the gaps. While in the top curve the presence of peaks and shoulders clearly witnesses the existence of two gaps, in the irradiated samples this evidence is lacking, due to a progressive broadening of the curves accompanied by a reduction in their height. The same happens in doped MgB₂^{7,24}. In all these cases, the existence of two gaps can be inferred from the fit of the curves with the BTK model or evidenced by the application of a magnetic field³. The BTK curves that best fit the experimental data are shown in Fig. 2 as solid lines. For all the curves in samples P0, P3 and P3.7, the two-band fit works better than the single-band one, since it reproduces both the width of the Andreev-reflection structures and the position of the peaks, while the single-band fit (dashed lines) does not.

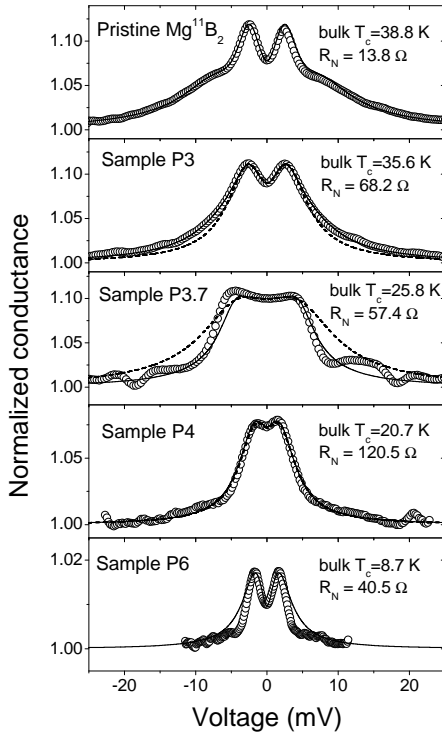


FIG. 2: Normalized conductance curves (symbols) of different point contacts on neutron-irradiated $Mg^{11}B_2$ polycrystals at $T=4.2$ K. The curves are labeled with the name of the samples and the relevant bulk T_c according to Ref.¹². The values of the normal-state resistance are also indicated. Solid lines are the best-fitting curves given by the appropriate BTK model (two-band in samples P0 to P4, single-band in sample P6). Dashed lines shown for samples P3, P3.7 and P4 represent the single-band best-fitting curve to be compared to the two-band fit. In the case of sample P4, solid and dashed lines are almost superimposed.

The curve measured in sample P4 admits both a single-band and a two-band BTK fit, that are almost equally good – as a matter of fact, dashed and solid lines are almost superimposed in this case. In sample P6, the dips at $|V| > |V_{\text{peak}}|$ modify the shape of the curve so that asking the model to fit the curve in this region is nonsense. In these conditions, the parameters of the BTK model should be adjusted so as to fit the conductance maxima and the zero-bias dip between them. The single-band BTK model is sufficient to accomplish this task very well (see the line in the bottom panel of Fig. 2). If a two-gap fit is tried, the values of Δ_π and Δ_σ turn out to be so close to each other to be practically identical. Hence, in this sample the existence of a single gap can be safely concluded, in agreement with the findings of Ref. 12.

The gap amplitudes extracted from the fit of the curves shown in Fig. 2 (and of other curves not reported here, measured in different contacts on the same samples) are plotted in Fig. 3 as a function of T_c^A (black symbols). In the region around 18-19 K, the gap amplitudes resulting from the *two-band* fit of the conductance curves are

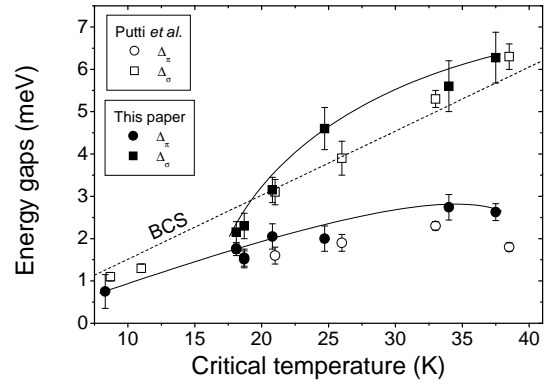


FIG. 3: Black symbols: gap amplitudes from PCS measurements, as a function of the Andreev critical temperature, T_c^A . Open symbols: gap amplitudes from specific-heat measurements¹² as a function of the critical temperature measured by specific heat. Solid lines are only guides to the eye, while the straight dashed line indicates the value of the gap for a conventional, BCS superconductor.

shown, but it should be borne in mind that a single-gap fit is possible as well in this region, giving a gap value $\Delta \simeq \Delta_\pi$. In the same figure, the gap amplitudes extracted from the fit of specific-heat measurements¹² are also shown (open symbols). The agreement between the two sets of data is very good in the whole range of critical temperatures, especially if one takes into account that: i) PCS is a local, surface-sensitive technique while specific heat is a bulk property; ii) the gap values obtained by PCS are correctly plotted versus the Andreev critical temperature of the contacts, T_c^A , while those taken from Ref. 12 are reported as a function of the specific-heat T_c .

The trend shown in Fig. 3 clearly indicates a transition from two-band to single-band superconductivity at high neutron fluences. That the heavily-irradiated material undergoes deep changes above a certain neutron fluence ($\Phi \simeq 10^{19} \text{ cm}^{-2}$) is confirmed by the steep decrease in T_c and B_{c2} , by the increase in the cell parameters a and c ^{11,13} and by the observed decrease in the σ -band DOS¹⁰. Incidentally, it is interesting to note the initial, small increase in Δ_π , which is the hallmark of an increase in the scattering between bands.

We tried to reproduce the experimental trend of the gaps Δ_π and Δ_σ reported in Fig. 3 within the two-band Eliashberg theory. A complete fit of the $\Delta_\pi(T_c^A)$ and $\Delta_\sigma(T_c^A)$ curves is actually impossible since in a certain range of critical temperatures both gaps are smaller than the BCS value (see Fig. 3) until a BCS-like gap ratio is almost recovered at $T_c \simeq 9$ K, when $\Delta \simeq 1$ meV. An energy gap smaller than the BCS value has indeed been observed in disordered, conventional superconductor²⁵ and the same might occur in a two-band system, but it is strictly forbidden within the Eliashberg theory and no explanation for these findings has been given yet. Once established this point, one can proceed with the fit.

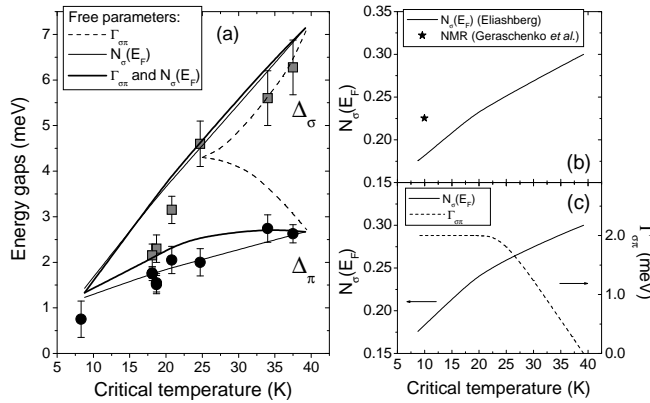


FIG. 4: (a) Symbols: gap amplitudes from PCS measurements, as a function of the Andreev critical temperature, T_c^A . Lines: gap amplitudes vs. T_c^A calculated by solving the two-band Eliashberg equations using as adjustable parameters: i) the interband scattering $\Gamma_{\sigma\pi}$ alone (dashed lines); ii) the σ -band DOS $N_{\sigma}(E_F)$ alone (thin solid lines); iii) both $\Gamma_{\sigma\pi}$ and $N_{\sigma}(E_F)$ (thick solid lines). (b) The $N_{\sigma}(E_F)$ vs. T_c curve necessary to fit the data (previous case (ii)). (c) The values of $N_{\sigma}(E_F)$ (left axis) and $\Gamma_{\sigma\pi}$ (right axis) necessary to fit the data of panel (a) (previous case (iii)).

The simplest approach is to consider the irradiated material as if it was only “disordered MgB₂”, thus neglecting the changes in the DOS, in the phonon frequencies and in the cell volume, and only increasing the interband scattering $\Gamma_{\sigma\pi}$. Once the value of this single parameter is chosen to reproduce the critical temperature of a given sample, no further degrees of freedom are left to reproduce the gap amplitudes. The resulting curves are shown in Fig. 4(a) as dashed lines. That increasing the interband scattering alone does not allow reproducing the experimental data is actually an expected result since, as previously pointed out, neutron irradiation has “side effects” such as sizeable changes in the σ DOS and in the cell parameters that are not included in this description.

The opposite approach consists in disregarding the effect of disorder (scattering) and only taking into account the change in the σ DOS at the Fermi level, $N_{\sigma}(E_F)$ ¹⁰. A reasonable fit of the experimental $\Delta_{\sigma}(T_c^A)$ and $\Delta_{\pi}(T_c^A)$ curves (with the general theoretical limitation that the gap ratios cannot be both smaller than the BCS one) is indeed obtained in this way, as indicated by thin solid lines in Fig. 4(a). That using a single parameter one can reproduce in such a good way the values of the two gaps *and* the critical temperature is, by itself, a good result and indicates that $N_{\sigma}(E_F)$ is largely dominant in determining the observed gap trend. This conclusion is consistent with the findings of Ref. 10 where the depression of T_c down to about 10 K was justified by inserting in the McMillan formula the reduced DOS (about 25% of the value in pristine MgB₂) measured by NMR. This single value is indicated by a star in panel (b) of Fig. 4, which also reports the T_c^A dependence of the σ DOS necessary to fit our PCS data (solid line).

The agreement between experimental data and the results of Eliashberg calculations can be slightly improved to account for the initial increase in Δ_{π} if both $N_{\sigma}(E_F)$ and $\Gamma_{\sigma\pi}$ are used as adjustable parameters. The resulting theoretical $\Delta_{\sigma}(T_c^A)$ and $\Delta_{\pi}(T_c^A)$ curves are reported as thick solid lines in Fig. 4(a), and the relevant behaviour of the parameters is indicated in Fig. 4(c). It is clear, however, that even including in the model all the possible effects of neutron irradiation, the agreement with the data can be hardly improved due to the aforementioned anomaly of the gap values that are both smaller than the BCS value in the T_c^A range between $\simeq 9$ K and $\simeq 20$ K.

IV. RESULTS IN ANOMALOUS CONTACTS

The percentage of “standard” contacts (as defined in the previous section) is equal to 100% in samples P0 and P3, but fast decreases in more irradiated samples. For example, it is about 70% in sample P3.7, 30% in sample P4 and becomes as small as 10% in sample P6. The remaining contacts are “anomalous” in the sense that their T_c^A exceeds T_c , which is clearly related to some kind of intrinsic or induced inhomogeneity in the samples. Fig. 5 reports the conductance curves of one of such anomalous contacts on the most irradiated sample (P6, bulk $T_c = 8.7$ K). The normal-state resistance of the contact was $R_N = 71 \Omega$. The temperature dependence of its conductance curve, reported in Fig. 5(a), clearly shows that the Andreev-reflection features persist well above the bulk critical temperature and disappear at $T_c^A = 32.7$ K, which is more than three times the bulk T_c measured by susceptibility. The thick line in Fig. 5(a) indicates the normal-state conductance curve. A fit of the low-temperature curve with the BTK model unambiguously shows the presence of two gaps with values similar to those obtained in standard contacts with the same T_c^A .

To further enlighten this point, we applied to the junction a magnetic field perpendicular to the direction of main current injection, and studied the behavior of the conductance curves on increasing the field intensity. In pure MgB₂, using a magnetic field allowed us to separate the partial contributions of the σ and π bands to the conductance across the junction^{3,14}. In doped MgB₂, the complete separation is not always possible but, if two gaps are present, an outward shift of the conductance maxima occurs when the smaller gap is strongly suppressed by the field^{7,26}. Fig. 5(b) reports the raw conductance curves of the same contact as in Fig. 5(a), measured in a magnetic field of increasing intensity. Again, the thick line corresponds to the normal-state conductance curve obtained here at $B = 6$ T (notice that it is identical to that of panel (a)). It is clearly seen that, at lower fields, the conductance peaks shift towards higher energies – a behavior that cannot be explained within a single-band model and arises from the stronger suppression of the π -band gap by the magnetic field³. The curves measured with $B = 0$ and $B = 2$ T are re-

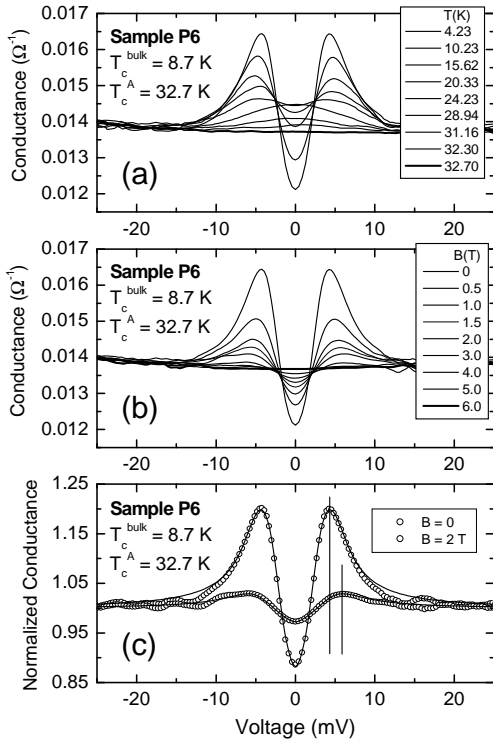


FIG. 5: (a) Temperature dependence of the raw conductance curves measured in a contact with $T_c^A=32.7$ K obtained on sample P6 (bulk $T_c=8.7$ K). The thick line is the normal-state conductance. (b) Magnetic-field dependence of the same conductance curve as in (a). Again, the thick line is the normal-state conductance. (c) Comparison of the conductance curves in zero field and in a magnetic field of 2 T. The outward displacement of the conductance peaks is highlighted by vertical lines.

ported, after normalization, in Fig. 5(c) together with the relevant two-band BTK fit. The shift of the conductance peaks is indicated by the two vertical lines. The values of the best-fitting parameters are the following: $\Delta_\pi = 3.38$ meV, $\Gamma_\pi = 1.35$ meV, $Z_\pi = 0.74$, $\Delta_\sigma = 5.00$ meV, $\Gamma_\sigma = 1.20$ meV, $Z_\sigma = 0.9$ for the zero-field curve; $\Delta_\pi = 0.6$ meV, $\Gamma_\pi = 2.05$ meV, $Z_\pi = 0.74$, $\Delta_\sigma = 4.85$ meV, $\Gamma_\sigma = 2.75$ meV, $Z_\sigma = 0.9$ for the curve in magnetic field. The weight w_π was taken equal to 0.8, as usual in polycrystalline samples.

Fig. 5 clearly shows that, apart from the high value of T_c^A , the anomalous contacts present very regular conductance curves, with a smooth dependence on magnetic field and temperature. Other examples of normalized conductance curves of anomalous contacts with T_c^A ranging from 35 K down to 22 K are reported in Fig. 6, together with the relevant two-band BTK fits. The agreement between experimental data and fitting curves is remarkably good. The gap amplitudes extracted from these fits (and from the fit of the curves in other anomalous contacts) are reported as a function of the local critical temperature T_c^A in Fig. 7 (black symbols). The behavior of the gaps measured in standard contacts is reported

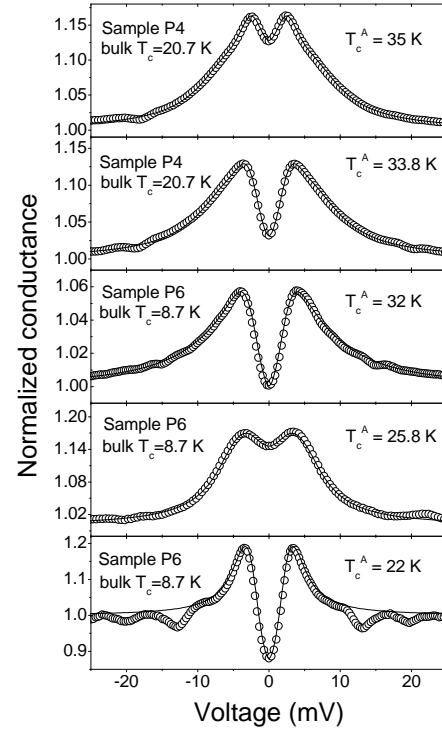


FIG. 6: Normalized conductance curves (symbols) of different anomalous point contacts on neutron-irradiated Mg^{11}B_2 polycrystals at $T=4.2$ K. The curves are labeled with the Andreev critical temperature T_c^A but the name of the samples and the relevant bulk T_c are also indicated. Lines are the best-fit curves given by the two-band BTK model.

for comparison (open symbols). It is clearly seen that, while the Δ_σ vs. T_c^A curve is rather similar in standard and anomalous contacts, the trend of Δ_π is fairly different. In anomalous contacts, the small gap Δ_π tends to remain constant or slightly increases on decreasing T_c^A , which generally indicates a substantial increase in the interband scattering^{8,9}. Extrapolating the experimental curves to lower critical temperatures suggests that the two gaps might tend to a common value of about 3 meV and reach it at a critical temperature of about 18 K, as in C-doped MgB_2 single crystals⁷.

The experimental trend of the gaps in anomalous contacts as a function of T_c^A can be analyzed within the two-band Eliashberg theory, as we did for standard contacts. Again, the first and simplest possibility consists in keeping all the parameters fixed to their values in pristine MgB_2 and simply increasing the interband scattering rate $\Gamma_{\sigma\pi}$ to simulate the disorder due to irradiation. The theoretical curves are reported in Fig. 8(a) as dashed lines, and the corresponding values of $\Gamma_{\sigma\pi}$ are shown in Fig. 8(b). As in standard contacts, the experimental values of Δ_π are incompatible with this simple picture. The next step towards a theoretical reproduction of the experimental data is to allow variations in the σ -band density of states at the Fermi level, thus using both $N_\sigma(E_F)$

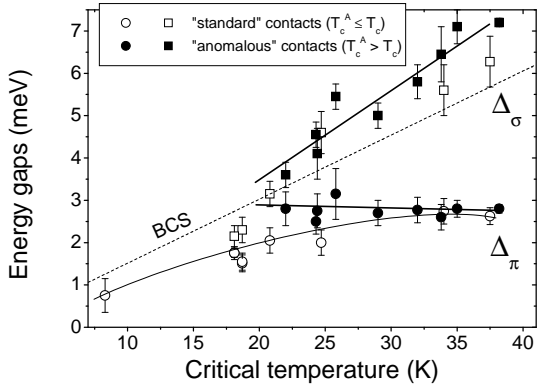


FIG. 7: Gap amplitudes from PCS measurements, as a function of the Andreev critical temperature, T_c^A , in anomalous contacts ($T_c^A > T_c$) (black symbols) compared to the gaps in standard contacts (open symbols). Solid lines are only guides to the eye, while the straight dashed line indicates the value of the gap for a conventional, BCS superconductor.

and $\Gamma_{\sigma\pi}$ as adjustable parameters to fit the experimental data. The best-fitting $\Delta_\sigma(T_c^A)$ and $\Delta_\pi(T_c^A)$ curves are reported in Fig. 8(a) (thick solid lines) while the values of the parameters are reported as a function of T_c^A in Fig. 8(c). The experimental gap values measured in anomalous contacts look to be quite well reproduced by taking into account the reduction in the σ -band DOS and the increase in interband scattering. The interesting point is that the values of $\Gamma_{\sigma\pi}$ necessary to fit the data in anomalous contacts are *higher* than those required to fit the gap amplitudes in standard contacts, as one can readily see by comparing Figs. 4(c) and 8(c). This is a consequence of the different behaviour of the small gap in the two cases and suggests that standard and anomalous contacts occur in regions of the sample with different degrees of disorder. Whether this inhomogeneity is intrinsic or is in some way induced by our point-contact technique is the subject of the following section.

V. POSSIBLE ORIGIN OF ANOMALOUS CONTACTS

Let us summarize here the properties of anomalous contacts that arise from the above.

1. Their critical temperature T_c^A , defined as the temperature at which the Andreev-reflection features disappear, is much greater than the bulk T_c (from 10 to 25 K more).
2. In these contacts Δ_σ is very similar to that measured in standard contacts with the same T_c^A , while Δ_π is a little greater indicating a possible enhancement of interband scattering.
3. The probability of finding anomalous contacts increases on increasing neutron irradiation.

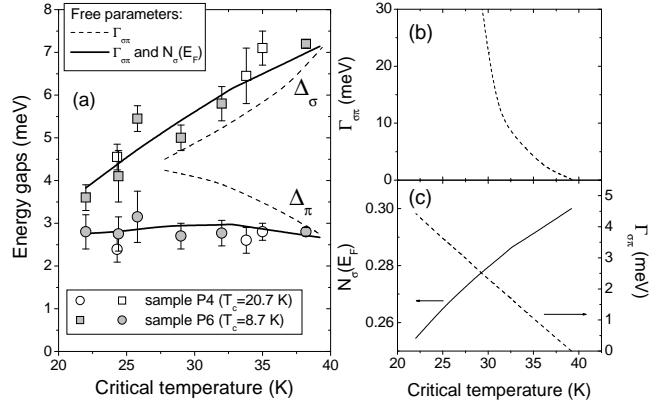


FIG. 8: (a) Gap amplitudes from PCS measurements in anomalous contacts (symbols), as a function of the Andreev critical temperature T_c^A . Open and filled symbols refer to sample P4 and P6, respectively. Lines: theoretical curves obtained within the Eliashberg theory by using only $\Gamma_{\sigma\pi}$ as adjustable parameter (dashed lines) or both $\Gamma_{\sigma\pi}$ and $N_\sigma(E_F)$ (solid lines). (b) The values of $\Gamma_{\sigma\pi}$ that give the dashed lines in panel (a), as a function of the critical temperature. (c) The values of $N_\sigma(E_F)$ (left axis) and $\Gamma_{\sigma\pi}$ (right axis) that give the solid lines in panel (a), as a function of the critical temperature.

Properties (1) and (2) might indicate that anomalous contacts are established in regions of the sample that are either less damaged or partially “reconstructed”, but in any case less disordered than the surrounding material. Point (3), however, rules out the former possibility so that anomalous contacts are most probably due to reconstructed regions. It has been shown in a recent paper²⁷ that heavily neutron-irradiated MgB₂ (with T_c as small as 5 K) thermally annealed at sufficiently high temperatures (up to 500 K) and long times (24 h) almost recovers all the characteristics (i.e. cell parameters, critical temperature, residual resistivity) of the pristine samples. In our case, there is no thermal treatment of the samples after irradiation, so one can wonder whether similar annealing effects can be due to the PCS measurements – i.e., because of the current locally injected in the sample through the point contacts – or from irradiation itself above a certain threshold dose. In the first case, no preexisting inhomogeneity in the samples has to be supposed (although very likely to be present) and the local reconstruction of the lattice previously disordered by irradiation is related (in some way to be clarified) to the PCS technique. In the second case, the samples should present locally annealed regions that are favored, due to their lower resistance, in the formation of the point contacts and thus determine their Andreev critical temperature. At this stage of our study, we cannot unequivocally decide in favor of one or the other hypothesis, (although different evidences point towards the former) and we will thus discuss both of them in the following sections.

A. Annealing induced by the PCS technique

Let us focus on the size of the contacts established between sample and Ag paint and refer for convenience to the contact made on sample P6 whose conductance curves are shown in the lower panel of Fig. 1. The normal-state resistance of this contact is $R_N = 40 \Omega$ and, as we already said, the shape of the curves (in particular, the presence of small dips¹⁷ and the offset of the curves on increasing temperature) tells us that the contact must be in the diffusive regime¹⁸. If only one contact was established between sample and counterelectrode, one could evaluate its radius a from the resistance R_N by means of the Wexler formula (eq. 1), in which we will approximate $\Gamma \simeq 1$. The calculation gives $a \simeq 90 \text{ \AA}$, which has to be compared with the effective mean free path $\ell \simeq 5 \text{ \AA}$ (which is actually closer to the *elastic* mean free path since it was evaluated from the residual resistivity) and with the coherence length $\xi \simeq 100 \text{ \AA}$ ¹³. None of the two conditions for spectroscopic analysis to be possible, i.e. $a \ll \ell$ (ballistic conduction) and $a \ll \xi$ would be fulfilled. In this situation, at bias voltages comparable to the energy gap, the carrier velocity would largely exceed the depairing value²³ and superconductivity would be destroyed in a region close to the contact of radius three times larger than ξ , with consequent loss of the Andreev signal. Of course this contrasts with the evidence of spectroscopic information present in the curves of Fig. 1 (c). Moreover, in these conditions the heating in the contact would be greater than experimentally observed. For example, using the standard equation valid for a circular aperture¹⁸

$$T_{\max}^2 = T_{\text{bath}}^2 + \frac{V^2}{4L} \quad (2)$$

one obtains that, for a total voltage drop of the order of V_{peak} , the temperature of the contact would reach the bulk $T_c = 8.7 \text{ K}$ when $T_{\text{bath}} = 6.5 \text{ K}$. This contrasts with the curves reported in Fig. 1 where the difference between T_c and T_c^A is less than 0.5 K. To reconcile the experimental findings with the value of the contact resistance, we are forced to admit that more than one contact is established between sample and counterelectrode. Actually, this is a rather natural assumption, considering the nature of our point contacts whose macroscopic area is about $2000 \mu\text{m}^2$. If the contact actually consists of parallel nano-junctions, each of them should have greater resistance than the parallel as a whole, so that, for example, ballistic conduction could be obtained even in contacts with fairly low macroscopic resistance. In our case, it can be shown that the existence of $N \approx 20$ diffusive contacts (supposed identical and with normal resistance $R_N = 800 \Omega$) can perfectly explain the observed heating in the contact region. In this case one obtains, *for each contact*, $a=8.2 \text{ \AA}$, and the temperature in the contact reaches the bulk T_c for $V = V_{\text{peak}}$ when $T_{\text{bath}} = 8.2 \text{ K}$. In addition, when the bias is of the order of magnitude of the gap, the current density j in the contact region

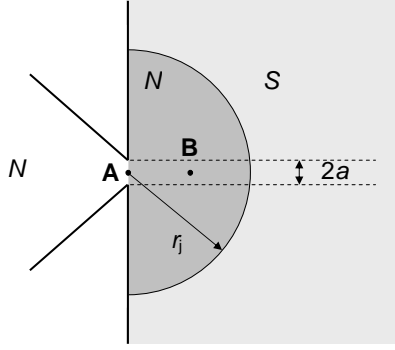


FIG. 9: Schematic representation of a point contact of radius a with the region of radius r_j driven normal by the current density, which exceeds the critical value in the vicinity of the striction. Points A and B are defined in the text.

is overcritical (take into account that in P6 $j_c \simeq 2 \cdot 10^5 \text{ A/cm}^2$ ¹¹) and the distance r_j in the superconductor over which j decays to the critical value (see Fig. 9) is of the order of $80 \text{ \AA} < \xi$ thus ensuring the spectroscopic properties of the contact.

Let us now recall that, whenever the contact resistance was too small or too high, or the conductance curve was unsatisfactory, or we simply wanted to change contact, we tuned the normal-state resistance by applying either currents or voltage pulses. What happens when such a voltage pulse (some Volts for $\simeq 20 \div 80 \text{ ms}$, as experimentally determined) is applied to the above mentioned contact? At this bias value, r_j is certainly greater than ξ so that a big normal region is formed in which a very intense current flows for a time of the order of few tens of milliseconds (see Fig. 9). This current gives rise to dissipation in this normal region that is then quickly heated above the bath temperature ($T_{\text{bath}} = 4.2 \text{ K}$). Let V be the total measured voltage drop between sample and counterelectrode, $V - V_0$ the voltage drop in the contact itself (which is supposed to be in diffusive regime) so that V_0 is the potential difference across the (hemispherical) normal region of radius r_j (see Fig. 9). Let us recall that r_j is the distance from the contact at which the current density decays to the critical value. If j_0 is the current density in the orifice, then at distance r from it one has

$$j(r) = j_0 \cdot \frac{a^2}{2r^2} \quad (3)$$

On the other hand, the current flowing through the contact is $I = (V - V_0)/R_{\text{PC}}$. Here, R_{PC} is the resistance of the point contact according to eq. 1 where, in the Maxwell term, $\rho(T)$ is the resistivity of the sample in the normal state, at the temperature it will reach in the contact region because of the Joule effect. Let us call ρ_{ave} the average of $\rho(T)$ in the temperature range to be determined (in sample P6 the RRR is so small that the value $\rho_{\text{ave}} \approx 160 \mu\Omega\text{cm}$ can be acceptable for a wide range of temperatures). Using these expressions one can

calculate the voltage drop across the normal region that is given by

$$V_0 = \frac{K \cdot V}{1 + K} \text{ where}$$

$$K = \frac{\rho_{\text{ave}}}{2\pi R_{\text{PC}}} \left(\frac{1}{a} - \frac{1}{r_j} \right). \quad (4)$$

Using eq. 3, one thus obtains

$$r_j = \sqrt{\frac{(V - V_0)}{2\pi R_{\text{PC}} j_c}}. \quad (5)$$

In our case (20 contacts, each with $a = 8.2 \text{ \AA}$) and for $V = 1 \text{ V}$, the solution of Eqs. 4 and 5 gives $V_0 = 0.257 \text{ V}$ and $r_j = 2576 \text{ \AA}$. The Joule effect in the normal region is expected to increase very much the local temperature, possibly giving rise to local annealing of the irradiated MgB_2 . One could wonder whether the temperature reached in the material is high enough to provoke annealing effects. Actually, we expect temperatures of the order of $1000 \text{ }^\circ\text{C}$ to be reached since, in some cases, we found out that the gold wire connecting the Ag spot to the pads of the sample holder had melted after this operation. The maximum temperature in the contact region (point A in fig. 9), evaluated from eq. 2 and from the voltage drop in the Maxwell part of the contact is $T_A \simeq 1300 \text{ K}$. The maximum temperature reached in the normal region (of radius r_j) driven normal by the current can be fairly simply evaluated by imposing that the thermal energy generated within the normal volume by heating effects equals the flux of heat current across the boundary. Unfortunately, the geometry of the boundary conditions and of the normal region in our case complicates the problem so that a correct evaluation requires finite-element calculations. However, one can approximate the problem and use a more convenient geometry, i.e. suppose that the volume is a cylindrical rod of length r_j and radius a . By assuming that the material follows the Wiedemann-Franz law and its resistivity is linear with temperature, and neglecting the heat flux through the side surface of the rod, we estimate the maximum temperature at the center of the rod (point B in fig. 9) to be $T_B \simeq 640 \text{ K}$. T_B turns out to be independent of r_j . This suggests that eq. 2, originally derived for a circular aperture¹⁸ might approximately hold in this case too. This approach gives the result $T_B \simeq 820 \text{ K}$. These estimated temperatures are all higher than those used by Wilke et al., even if the duration of the heating process is by far shorter. According to our results, annealing processes are most probable in the contact region, i.e. close to the physical interface between the two materials.

B. Irradiation-induced annealing

Annealing effects due to the irradiation itself can indeed occur, if irradiation takes place at low temperature,

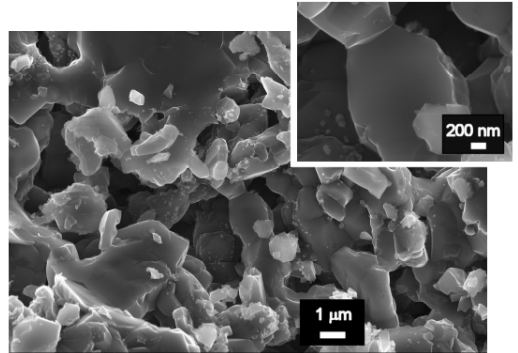


FIG. 10: FESEM image of the sample P6, showing the presence of rather large, well connected grains with smooth surface (see also the zoom in the inset).

because of the stimulated recombination of close Frenkel pairs²⁸. If, otherwise, irradiation is carried out at room temperature or above, the defects can migrate so that competing phenomena such as creation and annihilation of point defects or formation and coagulation of defect clusters can partly compensate each other²⁹, giving rise to saturation in some physical parameters. Similar phenomena are suggested, in our case, by the tendency to saturation in ρ_0 , T_c and the c axis¹¹ at very high neutron doses – being the other possible reason of saturation, i.e. the complete amorphization, ruled out by the sharpness of the X-ray peaks. Whatever the exact nature of the reconstruction process, locally-annealed regions should feature higher critical temperature than the remaining part of the sample, but since their presence is neither detected by susceptibility, nor by specific heat and resistivity measurements, they should represent a negligible part of the sample volume and should be imagined as isolated regions of small size. Moreover, if the macroscopic correlation between ρ_0 and T_c observed in irradiated and annealed samples^{11,27} is to be conserved also on a local scale, these regions are expected to feature higher conductivity and greater density of states than the surrounding matrix.

With these ideas in mind, we performed SEM and STM analysis at room temperature of the most irradiated sample, where the probability of finding anomalous contacts was the highest. Fig. 10 shows a FESEM morphological image (from secondary electrons) of sample P6 showing the presence of large, well connected grains with smooth surface, as also shown by the zoom on a single grain reported in inset. Z-contrast images (from backscattered electrons) were also recorded in the same region, as well as maps of the chemical species obtained by microprobe analysis. Note that the FESEM we used (Zeiss SUPRA 40) is equipped with a EDX SiLi detector sensitive to light elements (B included) and no trace of chemical species other than Mg and B were detected in the sample, thus excluding the possibility of chemical in-

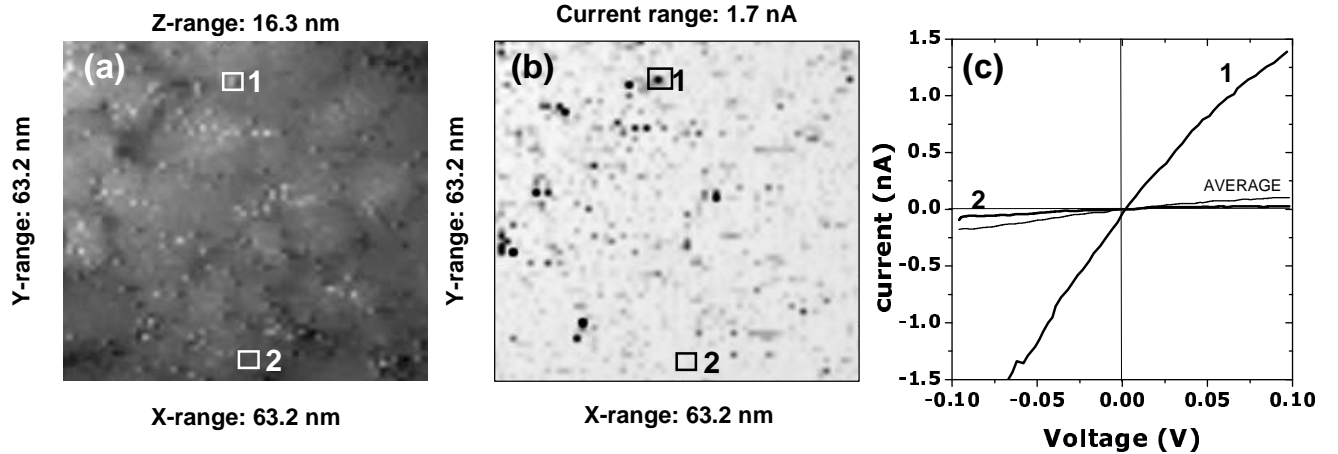


FIG. 11: (a) Scanning tunnel microscopy (STM) map of the surface of a single grain in sample P6, measured at room temperature. The map was taken with a fixed current equal to 2.0 nA. (b) Map of the current across the N-I-N junction (tip/air gap/sample) measured at constant tip-to-sample distance and constant voltage equal to 0.1 V. (c) I-V characteristics of the N-I-N tunnel junction in points 1 and 2 of the topographical image (a). The average I-V characteristic is also shown for comparison.

homogeneity (e.g. due to contaminations) on the sample surface. Owing to the relatively large size of the grains, we were able to perform scanning tunneling microscopy at room temperature on the surface of a single grain. The topographical image reported in Fig. 11(a) was recorded at a fixed current of 2.0 nA and shows the presence of rather smooth modulations on a length scale $\simeq 10$ nm in the xy plane and small brighter “dots” that look like protrusions. However, morphological SEM images on the surface of grains on a scale (100 nm \times 100 nm) comparable to that of Fig. 11(a) show absolutely no trace of such spots. The reason is that STM is sensitive not only to morphology, but also to the local density of states, i.e. regions with higher density of states appear brighter in the STM map because they give rise to a higher conductance across the tunnel junction. The topographical signal can be removed by performing a scan of the surface while keeping the tip-to-sample distance constant, i.e. operating in STS mode. The result is shown in Fig. 11(b) as a map of the current measured across the junction at constant tip-to-sample distance and constant voltage. For best clarity and to enhance the contrast, the color scale has been inverted here so that darker spots correspond to higher currents (the voltage between tip and sample is kept fixed at 0.1 V). A correspondence with the bright spots of Fig. 11(a) is clearly seen – while the smooth modulation is no longer observed. For further confirmation, Fig. 11(c) reports the I-V characteristics measured in two points (indicated by small squares in panels (a) and (b)) together with the average of the I-V curves measured in the whole region. It is clear that the “dots” observed in the STM maps represent very small regions (typically $\varnothing \simeq 1$ nm) with higher conductivity with respect to the surrounding material, that is exactly what one would expect for locally annealed regions with

higher critical temperature than the bulk.

However, these regions might be too small for superconductivity to develop in them when the surrounding matrix is in the normal state (while below the critical temperature of the matrix they are driven superconducting by proximity). According to the Anderson criterion for the size-effect in superconductors^{30,31}, in fact, superconductivity can persist in ultrasmall particles as long as the spacing of the discrete energy levels in them, due to the confinement of the quantum states, is smaller than the energy gap in the bulk. The spacing of the discrete energy levels δE in a nanoparticle turns out to be

$$\delta E = \frac{1}{N(E_F)}$$

being $N(E_F)$ the number of electron states per eV in the whole particle volume. In our case, $\delta E \simeq 43$ meV if one uses the total DOS of unirradiated MgB₂ (equal to 0.7 states /eV·cell, according to first-principle calculations³²) and a volume of 1 nm³. Note that this value for δE is already much greater than the gap and further increases if one takes into account the reduction in the DOS due to irradiation. Hence, particles of 1 nm³ cannot develop superconductivity. However, it is interesting to note that the minimum side of a cubic particle for the level spacing to be of order of the larger gap Δ_σ is about 2 nm. To be conservative, one can safely say that particles of 3-5 nm with a partly “reconstructed” lattice could be really superconducting above the bulk T_c . Some bright regions made up of clusters of point-like spots are actually observed in some part of the grain surface – possibly generated by some clustering mechanism during irradiation. The density of these regions is much lower than that of the bright dots in Fig. 11(a) and the problem then rises of why should they dominate the char-

acteristics of the macroscopic contacts made by using the Ag paint.

A partial answer to this question can be given, again, by the technique we use to tune the contact characteristics. What actually happens in the contact region when a voltage pulse is applied is unknown; it is very likely for our macroscopic Ag-paint contact to actually consist of parallel nano-junctions in the area of the Ag spot. A possible model of our macroscopic contact is a parallel of resistors (the nanoscopic point contacts, with resistances of several hundred Ohms) and capacitors formed between the sample surface and the Ag glue drop facing it. One could thus imagine that, when a voltage pulse is applied, local discharge effects occur in some capacitors when the voltage exceeds the dielectric strength of the insulator (maybe glue or helium), so that new contacts are established. It is possible that, in this process, regions with higher conductivity are privileged for the formation of new conduction channels, so that the resulting, new contact is dominated by the conductivity (and the critical temperature) of these regions.

C. Discussion

Both the proposed mechanisms of formation of anomalous contacts require the application of a voltage pulse, either to provoke the local annealing in the contact region or to select the preexistent regions with higher conductivity (and higher local T_c). Therefore, none of the arguments discussed in the previous sections can be applied to “as made” contacts. Looking for indirect support to our hypotheses, we checked all the contacts we studied during several months and we discovered that indeed *only “modified” contacts show anomalous characteristics*. The few standard contacts we were able to obtain in sample P6, for example (among which the one shown in Fig. 1(c)), were actually “as-made”. After the first modification of the contact by voltage pulses, only anomalous contacts were obtained. This suggests that one of the mechanisms described above could really explain the origin of the anomalous contacts. Incidentally, looking at Fig. 7 it actually seems that, whichever the mechanism is, it can remove the violation of the BCS rule for the gap ratio. As a matter of fact, the trend of the gaps in anomalous contacts is by far more “classic” and explainable within the Eliashberg theory, as also evidenced by the good fit of Fig. 8.

Deciding in favor of one of the two hypotheses discussed in Sections V A and V B is however not so straightforward.

The first picture, in which the PCS technique causes local annealing, perfectly fits all the experimental facts. First, it explains in a very natural and satisfactory way the occurrence of anomalous contacts *only* after tuning the contact resistance and, more important, accounts for the fact that no standard characteristics can be re-obtained after tuning. Second, the increasing-with-

fluence probability of finding these contacts can be easily explained by the greater concentration of defects that can annihilate on annealing. Third, the observed increase in the small gap with respect to standard contacts with the same T_c^A can be explained as being due to the persistence of some additional disorder even in the annealed regions. On the other hand, a perfect recovery of the pristine properties is not possible due to the very short duration of the thermal pulse. Within this picture, no preexistent inhomogeneities with higher T_c than the bulk are needed to explain the presence of anomalous contacts. The bright spots observed in Fig. 11 (which are certainly related to irradiation since they are completely absent in the unirradiated sample), would not necessarily play a role in the formation of anomalous contacts and might be interpreted as point defects due to fast neutrons or to the recoil of α particles and Li nuclei – but a detailed investigation of their actual nature and properties is still to be done and will be the subject of a forthcoming paper.

The second picture, in which preexistent regions with higher conductivity and density of states are selected by our PCS technique, is less satisfactory in some respects. First, it requires interpreting the nanometric spots observed by STS as partially reconstructed regions, less disordered with respect to the surrounding matrix. Moreover, these spots are too small to develop superconductivity, and only seldom form nanometric clusters, which could instead be superconducting with T_c higher than that of the surrounding material. The low density of these clusters makes it difficult to understand the very high probability of anomalous contacts in the most irradiated sample. Even the proposed process of “selection” of these regions when the voltage pulse is applied to the contact is not very well understood.

Therefore, the local annealing induced by the PCS technique appears to be the most likely process giving rise to anomalous contacts. However, the possibility of an *interplay* between the two effects (annealing due to PCS and preexistent inhomogeneities) cannot be excluded: local heating in the contact region might help the migration of defects and their clustering together with the partial re-arrangement of nuclei in the lattice disordered by irradiation.

VI. CONCLUSIONS

In conclusion, we have presented the results of a series of point-contact measurements in polycrystalline samples of neutron-irradiated $Mg^{11}B_2$. By using the soft point-contact technique developed for MgB_2 and related compounds, we were able to measure the dependence of the gaps on the local critical temperature of the contacts. The resulting trend is in very good agreement with the results of specific-heat measurements, especially in the most irradiated samples, and perfectly confirms the first observation of gap merging in undoped MgB_2^{12} . This is particularly important since the two techniques are com-

pletely different and probe the surface and the bulk of the samples, respectively. An analysis of the experimental gap trend within the Eliashberg theory shows that a major role is probably played by the decrease in the density of B_{xy} states, even if a substantial increase in interband scattering can be present as theoretically expected. A fit of the gaps is however not possible in the whole range of critical temperatures because in a certain intermediate region both the gaps are smaller than the BCS value.

A striking result, from the experimental point of view, was the occurrence of anomalous contacts with Andreev critical temperature higher than that of the bulk material. The percentage of these contacts increased on increasing the fluence and approached 100% in the most irradiated sample. Apart from the enhanced T_c^A , these contacts show no anomaly in the sense that their conductance curves are perfectly fitted by the two-band BTK model, and their temperature and magnetic-field dependencies are perfectly standard. However, while the values of the large gap extracted from the fit of these curves perfectly agree with those obtained in standard contacts with the same T_c^A , the small gap departs from the observed trend in standard contacts and shows a clear tendency to remain constant or even slightly increase. Within the Eliashberg theory, this can be due to a greater amount of interband scattering in anomalous contacts. Two pos-

sible origins of this anomaly have been discussed. The first hypothesis is that these contacts are due to a local annealing of the material caused by our measuring technique – in particular, by the way we use to tune the contact characteristics. The second is that these contacts are actually established in preexisting regions with local higher critical temperature than the surrounding material. The former picture is strongly supported by several experimental facts (for example the evidence that none of the “as-made” contacts presents anomalous T_c^A and no standard characteristics can be re-obtained after tuning the contact resistance). The hypothesis of local annealing due to the tuning of the contact resistance is thus the most convincing one, even though a cooperative interaction of the two phenomena cannot be ruled out at this stage since high-conductivity nanometric regions are actually observed by STS in the most irradiated sample.

We are indebted to Ruggero Vaglio for suggestions about the interpretation of anomalous contacts and to Pratap Raychaudhuri for enlightening discussion about heating in the contact region. Special thanks to Marina Putti for fruitful collaboration and help. This work was done within the PRIN Project No. 2004022024 and the INTAS Project No. 01-0617. V.A.S. acknowledges support by Russian Foundation for Basic Research (Proj. No. 06-02-16490).

¹ A. Gurevich, Phys. Rev. B 67, 184515 (2003).
² A.E. Koshelev and A.A. Golubov, Phys. Rev. Lett. 90, 177002 (2003).
³ R.S. Gonnelli *et al.*, Phys. Rev. B 69, 100504(R) (2004).
⁴ M. R. Eskildsen *et al.*, Phys. Rev. Lett. **89**, 187003 (2002).
⁵ Y. Bugoslavsky, Y. Miyoshi, G. K. Perkins, A. D. Caplin, L. F. Cohen, A. V. Pogrebnyakov and X. X. Xi, Phys. Rev. B **72**, 224506 (2005).
⁶ A.Y. Liu, I.I. Mazin and J. Kortus, Phys. Rev. Lett. 87, 087005 (2001).
⁷ R.S. Gonnelli, D. Daghero, A. Calzolari, G.A. Ummarino, Valeria Dellarocca, V.A. Stepanov, S.M. Kazakov, N. Zhigadlo, and J. Karpinski Phys. Rev. B 71, 060503(R) (2005).
⁸ J. Kortus, O. V. Dolgov, R. H. Kremer, and A. A. Golubov, Phys. Rev. Lett. 94, 027002 (2005).
⁹ G. A. Ummarino, D. Daghero, R. S. Gonnelli, A.H. Moudan, Phys. Rev. B 71, 134511 (2005).
¹⁰ A.P. Geraschenko *et al.*, Phys. Rev. B 65, 132506 (2002).
¹¹ M. Putti *et al.*, Appl. Phys. Lett. 86, 112503 (2005).
¹² M. Putti *et al.*, Phys. Rev. Lett. 96, 077003 (2006).
¹³ C. Tarantini *et al.*, Phys. Rev. B 73, 134518 (2006).
¹⁴ R.S. Gonnelli *et al.*, Phys. Rev. Lett. 89, 247004 (2002).
¹⁵ G.E. Blonder, M. Tinkham and T.M. Klapwijk, Phys. Rev. B 25, 4515 (1982).
¹⁶ A. Brinkman *et al.*, Phys. Rev. B 65, 180517(R) (2002); A.A. Golubov *et al.*, Phys. Rev. B 66, 054524 (2002).
¹⁷ Goutam Sheet, S. Mukhopadhyay, and P. Raychaudhuri, Phys. Rev. B 69, 134507 (2004).
¹⁸ A.M. Duif, A.G.M. Jansen and P. Wyder, J. Phys.: Condens. Matter 1, 3157 (1989).
¹⁹ G. Wexler, Proc. Phys. Soc. 89, 927-941 (1966).
²⁰ Yu.G. Naidyuk, I.K. Yanson, *Point-contact spectroscopy*, Springer Series in Solid-State Sciences, Vol. 145, 2004, XI.
²¹ K. Gloos, Phys. Rev. Lett. 85, 5257 (2000).
²² J. R. Walldram, Superconductivity of Metals and Cuprates, IOP Publishing, Bristol 1996.
²³ G. Deutscher, Rev. Mod. Phys. 77, 109 (2005).
²⁴ J. Karpinski, N.D. Zhigadlo, G. Schuck, S.M. Kazakov, B. Batlogg, K. Rogacki, R. Puzniak, J. Jun, E. Muller, P. Wagli, R.S. Gonnelli, D. Daghero, G.A. Ummarino, V.A. Stepanov Physical Review B 71, 174506 (2005).
²⁵ C. Camerlingo *et al.*, Phys. Rev. B 31, 3121 (1985); K. Tanabe *et al.*, Appl. Phys. Lett. 44, 559 (1984).
²⁶ R.S. Gonnelli, D. Daghero, G.A. Ummarino, A. Calzolari, M. Tortello, V.A. Stepanov, N.D. Zhigadlo, K. Rogacki, and J. Karpinski, Phys. Rev. Lett. 97, 037001 (2006).
²⁷ R. H. T. Wilke, S. L. Budko, and P. C. Canfield, J. Farmer, S. T. Hannahs, Phys. Rev. B 73, 134512 (2006).
²⁸ R. S. Averback and K. L. Merkle, Phys. Rev. B 16, 3860 (1977).
²⁹ E.V. Kolontsova, Usp. Fiz. Nauk 151, 149 (1987).
³⁰ P.W. Anderson, J. Phys. Chem. Solids 11, 26 (1959).
³¹ B. Mühlischlegel, D.J. Scalapino and R. Denton, Phys. Rev. B 6, 1767 (1972).
³² G. Satta, G. Profeta, F. Bernardini, A. Continenza, and S. Massidda, Phys. Rev. B 64, 104507 (2001).